Received: 21 June 2021 | Revised: 5 November 2021 | Accepted: 13 November 2021

DOI: 10.1002/rob.22050

RESEARCH ARTICLE

WILEY

Development and test of a Lunar Excavation and Size Separation System (LES^3) for the LUVMI-X rover platform

Gunter H. Just[1] | Matthew J. Roy[1,2] | Katherine H. Joy[3] | Gregory C. Hutchings[1] | Katharine L. Smith[1]

[1]Department of Mechanical, Aerospace and Civil Engineering, University of Manchester, Manchester, UK

[2]Henry Royce Institute, Department of Materials, University of Manchester, Manchester, UK

[3]Department of Earth and Environmental Sciences, University of Manchester, Manchester, UK

Correspondence

Gunter H. Just, Department of Mechanical, Aerospace and Civil Engineering, University of Manchester, Oxford Rd, M13 9PL, Manchester, UK.
Email: gunter.just@manchester.ac.uk

Funding information

European Space Agency; EPSRC Doctoral Training Partnership; Leverhulme Trust; The Royal Society; Science and Technology Facilities Council; FAIR-SPACE Hub

Abstract

Future sustained human presence on the Moon will require us to make use of lunar resources. This in-situ resource utilisation (ISRU) process will require suitable feedstock (i.e., lunar regolith) that has been both acquired and prepared (or beneficiated) to set standards. Acquisition of pre-processed regolith, is an often overlooked engineering challenge in the demanding and low-gravity environment of the lunar surface. Currently, regolith excavation and size separation are often developed independently of each other. Here, we present the Lunar Excavation and Size Separation System (LES^3), which is an engineered one-system solution to combine the acquisition of lunar regolith as well as separate it into two distinct size fractions, and therefore, can assist to define the quality of the feedstock material for ISRU processes. Intended for use with a lightweight (40–60 kg) lunar rover (LUnar Volatiles Mobile Instrumentation-X; LUVMI-X) currently under development, the mechanism utilises vibrations to reduce excavation forces and facilitate size separation. Low excavation forces are crucial for lunar excavators to be deployable on lightweight robotic platforms as limited traction forces are available. The rationale behind the mechanism is explained, its capabilities in the support of science and ISRU are showcased, and results from several laboratory test campaigns, including tests of gravitational dry sieving of different regolith simulants, are presented. The LES^3 can excavate up to 100 g in a single charge while maintaining excavation forces of less than 8 N and having a mass of less than 2 kg. Finally, areas of improvement for a second iteration of the design are presented and explained. The LES^3 proof of concept shows that combining of regolith excavation and size-separation in a single mechanism is feasible.

KEYWORDS

excavation, in-situ resource utilisation, lunar exploration, regolith, robotics, rovers

1 | INTRODUCTION

The Moon and its exploration have once again become an important aspect of most space agency roadmaps, which in turn acts as motivation for a multitude of private companies to develop launch vehicles, landers, and exploration technology (Chavers et al., 2016; Reddy, 2018; von Ehrenfried, 2020; Voosen, 2018). This refocus on lunar exploration comes to no surprise, as, even more than 50 years after the first lunar landing, there are many scientific questions remaining, ranging from the origin of the Moon, astronomy, and geology, to life sciences (Burns et al., 1990; Cockell, 2010; Crawford, 2004; Crawford & Joy, 2014; Crawford & Zarnecki, 2008; Crawford et al., 2012, 2016; Jaumann et al., 2012; Jester & Falcke, 2009; Joy et al., 2011, 2016; Neal, 2009). However, it is imperative not to rely on constant supply missions from Earth to enable a permanent human presence on the lunar surface as well as to develop technologies that can enable humankind's advance further into the Solar System (Ishimatsu et al., 2016). Using the locally available resources, referred to as in-situ resource utilisation (ISRU), is considered to be a crucial factor in achieving this aim (Anand et al., 2012; Carpenter et al., 2016; Crawford, 2015; Ellery, 2018; Larson et al., 2011; Lavoie & Spudis, 2016; Linne et al., 2015; Sacksteder & Sanders, 2007; Sanders, 2011; Sanders et al., 2008, 2010; Spudis & Lavoie, 2011). In the case of the Moon, the lunar soil (i.e., the surficial regolith) has proven to be a potentially viable feedstock for additive manufacturing and sintering processes (Balla et al., 2012; Cesaretti et al., 2014; Fateri & Gebhardt, 2015; Fateri et al., 2013; Goulas & Friel, 2016; Goulas et al., 2017, 2019; Labeaga-Martínez et al., 2017; Meurisse et al., 2017, 2018; Taylor et al., 2018), oxygen extraction (Balasubramaniam et al., 2010; Lomax et al., 2020; Sargeant et al., 2020; Schlüter & Cowley, 2020), as well as construction purposes (Hintze & Quintana, 2013; Lim et al., 2017; Raju et al., 2014; Sik Lee et al., 2015; Toutanji et al., 2005; Werkheser et al., 2015). Nevertheless, ISRU applications come at the end of the ISRU process chain (Hadler et al., 2020; Just et al., 2020b; Pelech et al., 2021), as material must be first excavated and subsequently beneficiated, for example, in the form of grain size separation. These two crucial steps are often oversimplified, yet, their successful integration is crucial to future lunar ISRU activities.

Most ISRU applications that are currently under investigation in a terrestrial laboratory setting use regolith analogues or simulants which have been sieved to a certain particle size distribution (PSD) before experiments are conducted (Taylor et al., 2016). While a process requiring a well-defined PSD or a small maximum particle size is relatively simple to achieve in a laboratory on Earth with different methods like wet and dry sieving, it becomes challenging in a lunar environment. In most publications detailing ISRU applications, this fact is not acknowledged and having access to a preprocessed feedstock is assumed a given. Table 1 shows an overview of certain ISRU applications and the level of reported feedstock preprocessing.

Table 1 shows that most potential end-users of excavated regolith material rely on or benefit from a certain level of size separation. Currently, excavation and size separation are usually considered as two independent steps in the ISRU process chain (see Just et al., 2020b or Hadler et al., 2020, for more details on the ISRU process chain), requiring regolith transport between the different processing sites or mechanisms. Thus, the development of a mechanism combining regolith excavation and beneficiation into one system seems highly beneficial. The development of the Lunar Excavation and Size Separation System (LES^3) was driven by this aim, about which there are currently few detailed published studies available. Second, we present the results of an investigation of gravitational dry-sieving of regolith, an area where little experimental data is available.

2 | THE LUVMI-X ROVER PLATFORM: SCIENTIFIC AND ISRU OBJECTIVES ENABLED BY LES^3

LUVMI-X is a small and lightweight four-wheeled lunar rover currently under development by Space Applications Services (Garcet et al., 2019; Losekamm et al., 2021), of which a rendering can be seen in Figure 1. The rover has a total mass of 40–60 kg, and a total payload capacity of 24 standard units (U) (1 U ≈ 10 × 10 × 10 cm; Gatsonis et al., 2016), split into 12 U per payload bay (front and back of the rover). Therefore, any payload mechanism must be storable within this envelope for launch. The ground clearance of ~30 cm when roving can be lowered to ~10 cm with the use of its suspension, allowing mechanisms to be deployed closer to the lunar surface, reducing the necessary reach, and thus structural mass. Due to its low mass, the rover can only provide a limited amount of effective traction force, requiring any excavation subsystem to operate with minimal excavation forces.

The development of a low-mass and low excavation force mechanism capable of excavating and size separating the lunar regolith is the objective of the presented study. When incorporated into LUVMI-X, the LES^3 will have three main functions in support of scientific as well as ISRU activities on the lunar surface:

- **Excavation and feedstock beneficiation:** Two distinct size fractions of regolith feedstock can be delivered to different ISRU processes, which is beneficial to the process control and product quality of a multitude of ISRU applications, like for instance additive manufacturing, regolith sintering, or oxygen extraction (see Table 1).
- **LIBS support:** For compositional analysis of the lunar surface, LUVMI-X carries a laser-induced breakdown spectroscopy (LIBS) system on-board (VOlatiles Identification by Laser Ablation

TABLE 1 Overview of ISRU processes and the size fraction of regolith analogues/simulants used for laboratory tests

Process	Analogue/ simulant	Size fraction	Reference	Comments
Additive manufacturing				
Selective laser melting	JSC-1A	<125 μm	Goulas et al. (2019)	Sieved
	JSC-1A	<125 μm	Goulas and Friel (2016)	Sieved + Dried
	JSC-1A	<63 μm	Fateri and Gebhardt (2015)	Sieved; Raw material showed heterogeneous structure
	JSC-1A	<200 μm	Fateri et al. (2013)	Sieved
	NU-LHT-2M	<150 μm	Sitta (2017)	Sieved
	N.A.	~20–50 μm	Terrestrial: metal powders; (Song et al., 2020)	Round particles
Direct energy deposition	JSC-1AC	50–150 μm	Balla et al. (2012)	Sieved
Regolith ink 3D printing	JSC-1A	<50 μm	Jakus et al. (2017)	Sieved
Additive manufacturing with light-reacting binding agent	EAC-1A	8 μm	Altun et al. (2021)	Milled
Sintering				
Solar sintering	JSC-1A & 2 A	<1000 μm	Meurisse et al. (2018)	Simulant as received + Sieved
		<400 μm		
Sintering	JSC-1A	25–1000 μm	Meurisse et al. (2017)	Simulant as received
Regolith ink sintering	JSC-1A	<50 μm	Taylor et al., (2018)	Sieved
Microwaves	JSC-1A & MLS-1	N.A.	Allan et al. (2013), Taylor and Meek (2005)	Bulk simulant
Selective separation sintering	JSC-1A	N.A.	Zhang and Khoshnevis (2015)	Assumed similar to SLM
Large scale construction				
Contour crafting (sulfur)	JSC-1A	N.A.	Khoshnevis et al. (2016), Werkheser et al. (2015)	Bulk simulant
Regolith concrete	N.A.	<75 μm	Sik Lee et al. (2015)	Milled
Oxygen extraction				
Metalysis-FFC (Fray, Farthing, Chen)	JSC-2A	>53–1000 μm	Lomax et al. (2020)	Sieved
Hydrogen reduction	NU-LHT-2M	Small particles advantageous	Sargeant et al. (2020), comm.[a]	Bulk simulant
Carbothermal reduction	MLS-1 & JSC-1	N.A.	Gustafson et al. (2011)	Bulk simulant
Other				
Magnesium combustion	JSC-1A	~6 μm	Delgado and Shafirovich (2013)	Milled

Note: Comment column indicates how this level of preprocessing was achieved. For methods labeled N.A., no information could be obtained and if the comment states "Bulk simulant", no requirement regarding the particle size was found. The statement presented for hydrogen reduction with the label "comm." was obtained in private communications with the researcher of the published work.

[a]H. Sargeant, Open University (UK).

(VOILA)) (Garcet et al., 2019; Losekamm et al., 2021; Vogt et al., 2020, 2021). Our proposed excavation method will be able to scrape/trench into the surface of the lunar regolith, revealing subsurface rock and soil samples available for LIBS investigations. Therefore, soils of interest or specific soil features, such as water content, can be investigated in more detail or at different depths (Lasue et al., 2012).

- **Geotechnical properties of regolith:** High-resolution images of the excavated trenches, as well as the two size fractions within their storage containers or excavated piles can provide

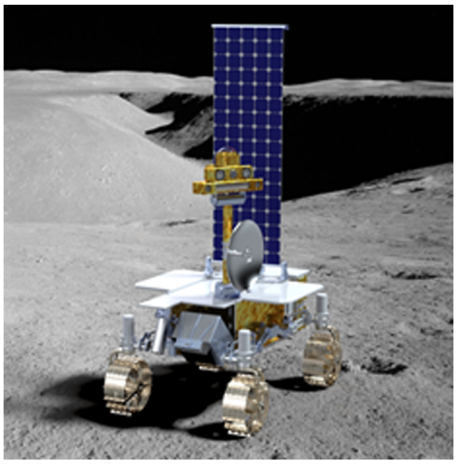

FIGURE 1 Rendering of the LUVMI-X rover platform on the lunar surface. Image credit: Space Applications Services (publicly accessible at: https://www.h2020-luvmi-x.eu/gallery-page/) [Color figure can be viewed at wileyonlinelibrary.com]

information about the particle size distribution as well as physical properties of the soil, such as friction angles and cohesion (by measuring the angle of repose; for more detailed descriptions of these techniques, see Moore et al., 1999; Sullivan et al., 2011). Additionally, these strength parameters can also be calculated from the recorded excavation forces (Kobayashi et al., 2006).

Here, it is important to differentiate between a sampling/excavation mechanism intended to support analytical scientific research, like, for example, drill excavation as used in ESA's PROSPECT payload (Sefton-Nash et al., 2018), and a mechanism for which the sole purpose is to support ISRU activities, such as we propose for LES^3. For the former, cross-contamination of different sampling locations is an important issue that must be addressed and mitigated. The presented mechanism on the contrary, is intended and designed to support ISRU applications such as additive manufacturing or oxygen extraction, where cross-contamination of samples is less important. While LES^3 is directly capable of performing the first presented function, it supports the remaining two functions indirectly by excavating soil and its subsequent imaging.

3 | DESIGN AND DEVELOPMENT OF LES^3

3.1 | Working principle

The working principle of LES^3 consists of four main steps, which can be seen illustrated in Figure 2 and which will be explained in more detail below:

1. **Accumulation of soil:** After the arm has been lowered, the rover pushes the inlet through the soil at a shallow angle (here 15 degree), as shallow angles have been proven to result in low excavation forces (Just et al., 2021). Both outlet ports are blocked by spring-loaded gates and the vibration motor is operating. After a sufficient time, indicated by the front area of the inlet being filled with regolith or an increasing surcharge mass, the vibration motor (details of vibration in Section 5) stops, and the mechanism moves into Position 2—the pre-separation phase.
2. **Preseparation phase**: Since not all material is being pushed through the front sieving plate in Position 1, the second step is to pre-separate larger rock fragments (first step of size separation). In this position, which orientates the front sieving plate horizontally, both spring-loaded gates are still closed, and the vibration motor starts operation to facilitate size separation. Once there is no more material present on top of the screen, the vibration motor stops, and the mechanism moves into Position 3 where both the inlet and arm are at the same angle of ~45°.
3. **Sieving of fine fraction:** The spring-loaded gate for the fine fraction is actuated by the cam profile based on the inlet position, which allows the fines to exit the outlet port and fall through the arm into the storage container. The cam profile is optimised to open the gate slowly at the beginning (to minimise material loss) and faster once the connection of inlet and arm is almost made. The vibration motor is running to facilitate size separation. This operation continues until no more fines are registered entering the storage container (by means of a loadcell in the storage container), which stops the motor. Optionally, the arm can be moved back and forth to facilitate the separation process and prevent consolidation of the soil in the sieve (see Section 4). The coarse particles remain inside the inlet and the mechanism moves into Position 4, where the inlet is rotated ~110° back.
4. **Disposal of coarse fraction:** While rotating the inlet backwards, the spring-loaded gate for the fines closes as the cam profile disengages. Then, the other cam profile engages the second spring-loaded gate for the coarse fraction and opens it as the port aligns with the chute on the arm. Once in this position, the vibrating motor is activated, and the coarse particles fall into the chute. Again, once no more mass increase in the storage container is registered, the operation is considered completed and the mechanism is now ready for an optional cleaning Step 5, or the next regolith cut (extraction).
5. **Cleaning (optional):** If a decrease in separation efficiency is observed, the arm and inlet can be put into Position 5 which enables dislodging any remaining material. Here, the rover raises its suspension up to allow the arm to point downwards without touching the soil (angle variant, based on geography). The vibration motor engages and dislodges accumulated soil particles. The process can be accelerated by moving the arm up/and down, shaking the overall system.

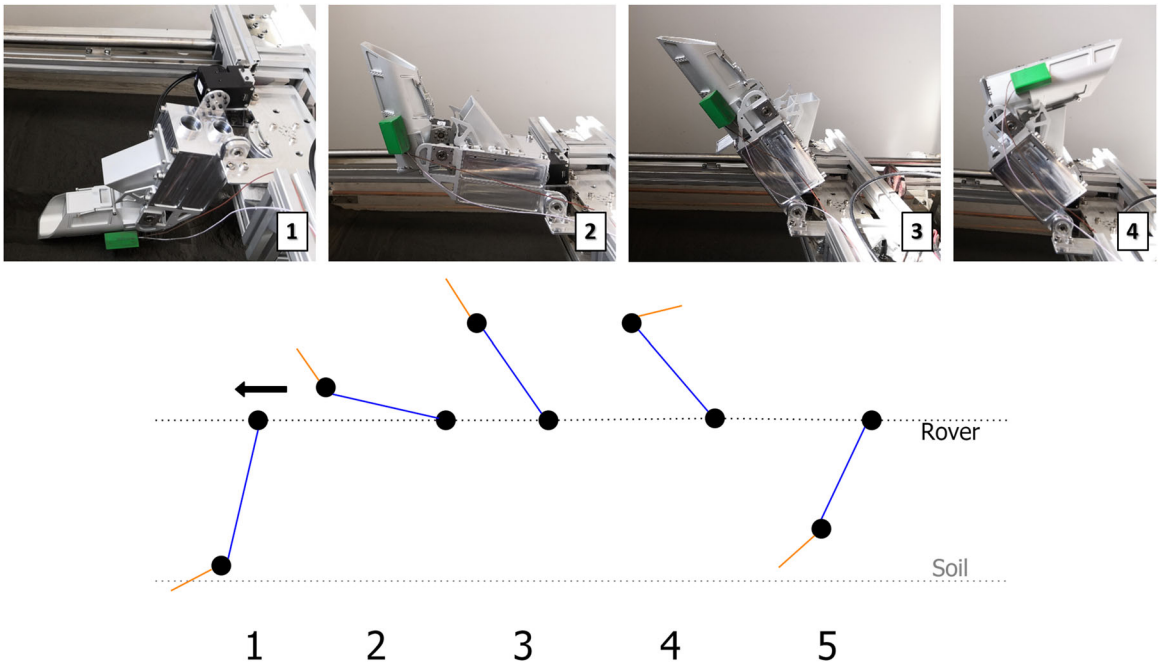

FIGURE 2 Illustration of the working principle of the LES^3 mechanism in a lab environment (top) and as a schematic (bottom). The inlet is held in orange, the arm is blue, and black dots signal rotational axes. Rover as well as regolith planes are indicated. Soil is accumulated using the inlet system (1), pre-separated (2), the fine fraction is separated (3), and the coarse fraction is removed from the inlet (4). The illustration at the bottom shows and additional cleaning step (5). Videos of the mechanism in operation can be found at https://doi.org/10.48420/14511480, https://doi.org/10.48420/14510535, https://doi.org/10.48420/14511477, and https://doi.org/10.48420/14511483 [Color figure can be viewed at wileyonlinelibrary.com]

3.2 | Mechanism design

The system consists of three distinct parts: The inlet or leading edge, the arm, and the base. The latter's design is expected to change, as the design of the turret is heavily depended on the way the mechanism will be integrated into the rover platform and the storage location for the excavated materials; specifications that are still being defined by the rover team at the moment. Thus, this part will only be discussed briefly in this publication. Figure 3 shows a CAD "sliced" view of the inlet (Figure 3 (III)) next to two views of the prototype (Figure 3 (I) and (II)) in a lab environment.

The excavation mechanism is based on a cylindrical inlet (see Figure 3 feature a; diameter ~50 mm; length ~130 mm), as this geometry resulted in the lowest excavation forces and little accumulation of surcharge during experiments performed by the authors in a large regolith analogue test bed at the University of Manchester (Just et al., 2021). A coarse mesh/sieving plate (see Figure 3 feature b; aperture size discussed in Section 5) separates out larger rock fragments and, therefore, acts as the first stage of regolith size separation. A finer mesh/sieving plate (see Figure 3 feature h; aperture size discussed in Section 5) will provide a second size separation step, leading to the creation of two distinct particle size fractions within the mechanism. Outlets for the coarse fraction (see Figure 3 feature c) and the fines (see Figure 3 feature d) are covered with spring loaded gates (see Figure 3 features e and f). A vibration motor (see Figure 3 feature g; Precision Microdrives 320-105), housed in a 3D-printed containment (see Figure 3 feature k; PLA), will facilitate excavation and size separation. The inlet is actuated by a high-torque stepper motor (see Figure 3 feature l; Dynamixel XM430-W350) and can rotate ~135 degrees around its connection point. The spring-loaded sliding gates are actuated by cam profiles (see Figure 3 features i and j) to keep the system as passive as possible and are equipped with small roller bearings (see Figure 3 feature m) to reduce necessary actuation forces and acting towards preventing kinematic locking.

The coarse size fraction will enter the arm through a chute (see Figure 4 feature n) on top of the arm which connects with the outlet (Figures 3 and 4 feature c). The regolith fines will enter the arm through a port that connects flush with the other outlet (Figure 3 feature d). Both size fractions will be guided back to the storage unit, located within the rover, inside the arm, which is divided horizontally into two channels/slides (Figure 3 feature o); vibrations will facilitate this transport, similar to a terrestrial vibrational conveyor. The design of the storage containers is subject of future work, as this task is dependent on the finalised mission design and intended integration location for the mechanism on the rover. The hollow shell structure of the arm minimises structural mass and can provide shielded and dust-proof locations for cabling and electronic components. Figure 5 displays details of the cam profiles (Figure 3 features i and j) and spring-loaded gates (Figure 3 features e and f). The arm is actuated by another high-torque stepper motor (p; Dynamixel XM540-W270) and attached to a base that acts as a turret with a third high-torque

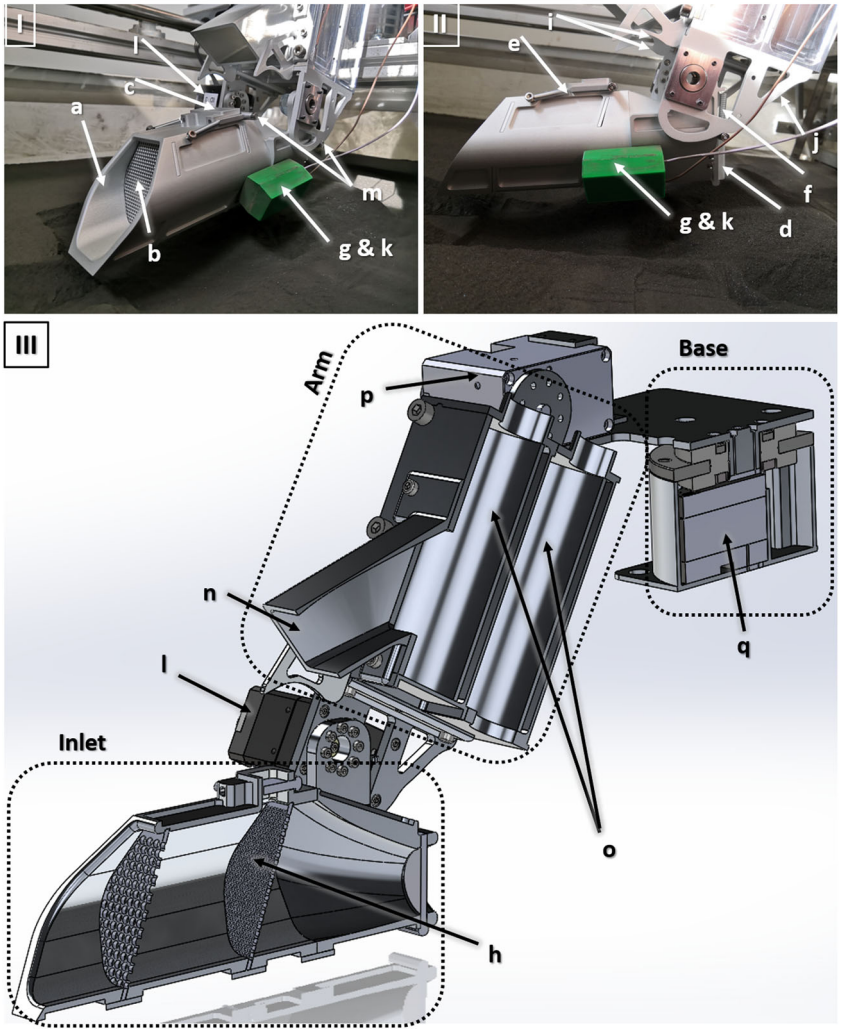

FIGURE 3 Mechanical design of the described prototype. Features I and II show the inlet with all its components in a laboratory environment and feature III presents a sliced 3D rendering of the whole mechanism with an indication of the three main parts. Individual components are: (a) cylindrical inlet, (b) coarse mesh/sieving plate, (c) outlet for coarse fraction, (d) outlet for fine fraction, (e and f) spring loaded gates, (g) vibration motor, (h) fine mesh/sieving plate, (i and j) cam profiles, (k) vibration motor containment, (l) high-torque stepper motor for inlet actuation, (m) roller bearings, (n) chute for coarse fraction, (o) channels/slides for two size fractions, (p and q) high-torque stepper motors for arm and base actuation. Videos of the mechanism in operation can be found at https://doi.org/10.48420/14511480, https://doi.org/10.48420/14510535, https://doi.org/10.48420/14511477, and https://doi.org/10.48420/14511483 [Color figure can be viewed at wileyonlinelibrary.com]

stepper motor located inside the base (q; Dynamixel XM430-W350). Therefore, the mechanism can be actuated in three active degrees of freedom in a yaw–pitch–pitch configuration, useful both for storing the mechanism during launch as well as to maximise its application possibilities. This assembly can be seen in Figures 3 and 4. For this first prototype all parts were machined from aluminum for its ease of manufacturing.

To support the evaluation of geotechnical regolith data, the LES^3 is equipped with a 20 MP color FLIR Blackfly camera (Figure 4 feature r), which is attached to the side of the arm with two degrees of freedom. The 3D-printed pan and tilt platform (Figure 4 feature s; ABS) is operated by two small servo motors (Figure 4 feature t). This not only enables observations of the inlet while excavating, but also allows closer examination of the surrounding area or the rover due to the adjustable focal length of the lens (Figure 4 feature u). The platform is additionally equipped with a range finder (Figure 4 feature v; Sharp GP2Y0A41SK0F), which allows the mechanism to verify the digging depth by pointing the sensor perpendicular to the surface. More specifications of the mechanism, such as mass, power consumption, and excavated mass per scoop, can be found in Section 5, as they have been verified during the testing phase.

4 | DRY SIEVING OF REGOLITH

In principle, LES^3 utilises a two-stage vibrating sieve to achieve the necessary level of size separation. Dry gravitational separation of regolith is often considered challenging (Rasera et al., 2020), and more complex separation techniques, such as electrostatic or magnetic separation, are proposed instead. While there are several publications on the separation of granular matter by means of vibration in a terrestrial setting (Kudrolli, 2004; Li & Tong, 2015; Wen et al., 2015), there is a very limited number of experimental studies available which investigate dry sieving of regolith or its simulants/analogues (Wilkinson, 2011; Williams et al., 1979). It may be challenging to achieve separation down to very small particles in the challenging low-gravity lunar conditions and due to the cohesive nature (Mitchell & Houston, 1972) and electrostatic charging (Colwell et al., 2007) of the regolith. However, gravitational size separation offers a considerably simpler way of achieving a basic level of size separation and has been successfully deployed in the Mars Science Laboratory's Collection and Handling for In situ Martian Rock Analysis (CHIMRA) mechanism (Sunshine, 2010); thus, its utilisation should not be ruled out categorically for lunar applications.

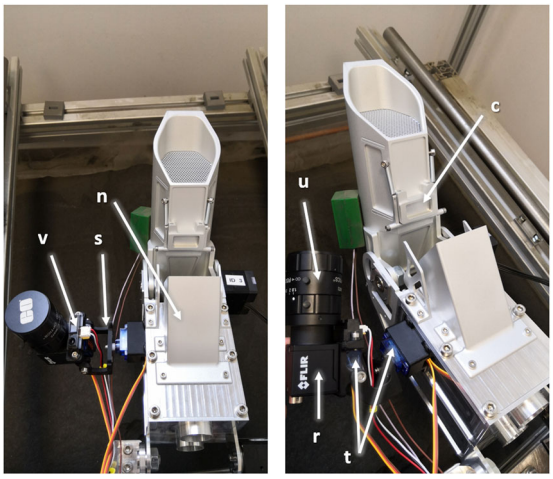

FIGURE 4 A detailed view of the connection between inlet and robotic arm, including a high-resolution camera mounted on a servo-actuated pan/tilt platform. Individual components are: (c) outlet for coarse fraction, (n) chute for coarse fraction, (r) 20 MP color FLIR Blackfly camera, (s) pan and tilt platform for camera, (t) two small servo motors for pan and tilt, (u) lens with adjustable focal length, (v) range finder. Videos of the mechanism in operation can be found at https://doi.org/10.48420/14511480, https://doi.org/10.48420/14510535, https://doi.org/10.48420/14511477, and https://doi.org/10.48420/14511483 [Color figure can be viewed at wileyonlinelibrary.com]

4.1 | Dry sieving experimental set-up and methods

To inform a realistic level of size separation and, thus, define the aperture size for the proposed LES[3] excavation mechanism as well as to understand the time required to perform such separation, a standardised stand-alone dry sieving experiment was conceptualised. The decision to perform this experiment as a stand-alone test is beneficial to the overall ISRU community, as the findings are not only applicable to the presented mechanism design but can inform decisions for a multitude of applications where regolith size separation is required. Figure 6 shows the experimental setup for this test. The rack is based on a support structure made of extruded aluminum profiles (Figure 6 feature a), which holds a 3D-printed platform (Figure 6 feature b; PLA). Standard 100 mm diameter woven-wire mesh test sieves (Figure 6 feature c; Glenammer; manufactured in accordance with B.S. 410/I.S.O. 3310 (British Standard Institution, 2000) and ASTM E11:20 (ASTM International, 2020) are held therein with four 3D-printed clamps (Figure 6 feature d; PLA). Underneath the sieve, a funnel (Figure 6 feature e; Fisher Scientific FUNSS100H) catches the separated fines and guides them into a weighing container (Figure 6 feature f), which is covered with a lid to minimise dust creation. The container rests on a scale with a beam loadcell (Figure 6 feature g; Phidgets CZL616C), which reports the separated mass as a function of time. A vibration motor (Figure 6 feature h; Precision Microdrives 320-105) is attached to a 3D-printed collar (Figure 6 feature i), which secures it tightly onto the sieve in a repeatable way. For this proof-of-concept the motor is operating at 2.5 V, resulting in an acceleration of 4.5 g and a frequency of around 90 Hz. A 3-axis accelerometer (Figure 6 feature j; MPU 6050) reported the vibrational intensity and ensured the consistency of the vibrations. All data was recorded at 2 Hz.

Four different analogue materials were tested, to get an understanding of how particle shape and other material properties, for instance density or particle cohesion, affect the outcome and to allow for a more robust estimation of the feasibility of the intended application. The chosen analogue materials were UoM-B (a complex ferro-silicate) (Just et al., 2020a), TUBS-M and TUBS-T (basalts) (Linke et al., 2018), as well as Hess Pumice Grade 1/0[1] (pumice powder), whereas each experimental run was performed with 200 g of the material; for a full characterisation and details regarding the PSD of analogue materials see the cited references. After weighing out the material in a beaker, it was added to the vibrating sieve. To ensure the repeatability of the runs and to make sure the experiment was not ended prematurely, an automated cut-off criterium was introduced. If the five-step rolling average of the mass increase of the fine fraction was below 0.07 % of the total analogue mass (equal to 0.14 g), the measurement would be flagged within the data acquisition code. If, during 240 consecutive measurements (equal to 2 min) of the experiment, 235 or more measurements were flagged, the experiment was considered as "potentially over". If during the next 240 measurements 235 or more potential termination criteria were recorded, the experiment was ended, as no more recordable change in separated mass was to be observed. This method was applied to not underestimate the importance of small regolith particles in any ISRU application, where separation can take a considerable amount of time as the experiment gets closer to the separation limit. In other words, a long linear increase with a very shallow slope can add up to an appreciable mass. This becomes important for applications which require a particle size distribution larger than a certain cut-off, as too many fine particles in the feedstock can here reduce the quality of the ISRU product, cause an increased demand of consumables, or damage components, such as filters. After the experiment, both size fractions were weighed and the lost mass calculated. For all initial tests, sieves were cleaned with a sieve brush in between runs.

4.2 | Dry sieving experimental results

All performed experimental runs, including aperture size, used analogue, total analogue mass, mass of coarse/fine fraction, mass of lost material, percentage of passed material, expected percentage of passing based on the particle size distribution, as well as the required time to meet the end criterium (i.e., residence time) can be found in Table 2. Since the particle size distribution of the used analogue materials is very different, not all analogues were tested with all aperture sizes. For example, UoM-B has a nominal particle size distribution up to 125 microns (for details see Just et al., 2020a), and,

[1]Idaho, USA; full details and material data sheet available at: https://hesspumice.com/

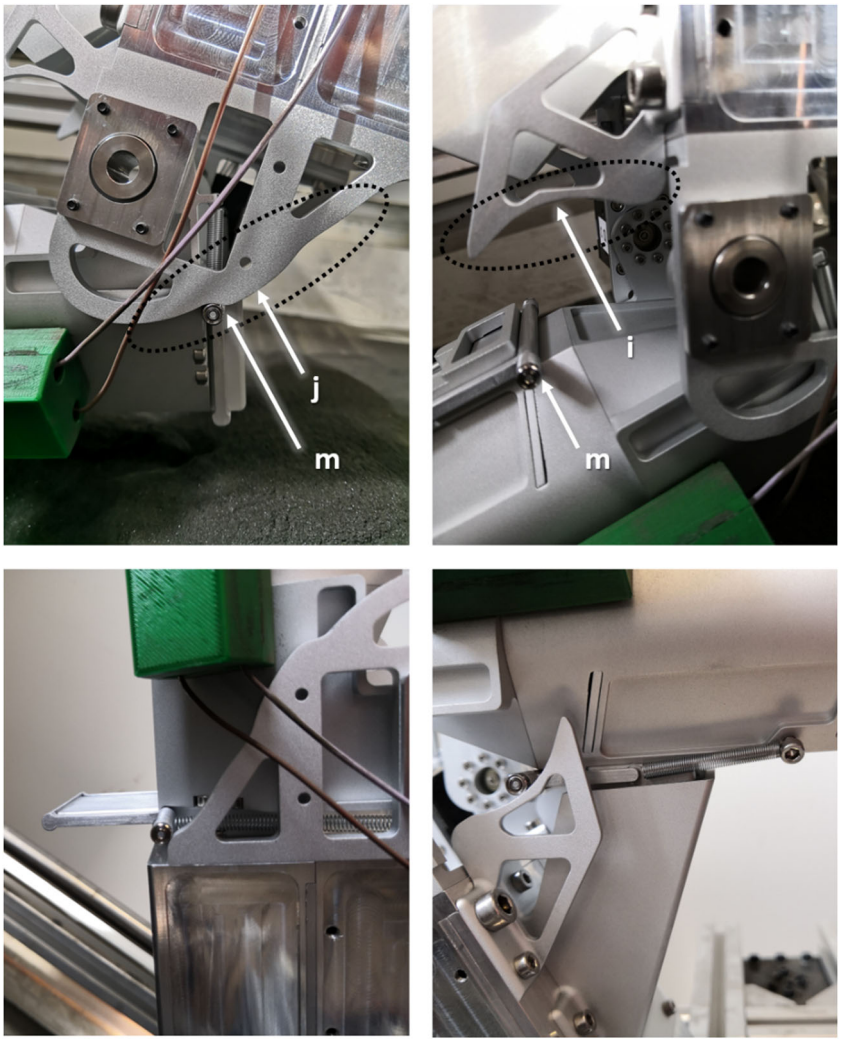

FIGURE 5 Details of the cam profiles required for actuation of the spring-loaded gates (with roller bearings [m]) for both fine (j; top left) and coarse fraction (i; top right). The bottom images show both cam profiles with a fully engaged follower [Color figure can be viewed at wileyonlinelibrary.com]

thus, using a sieve with an aperture coarser than 500 microns is untenable when considering the residence time. For the two data sets that are greyed out in Table 2, the residence time was interpolated based on their particle size distribution passing value due to the immense increase in time demand.

Figure 7 shows two images during operation of the experiment with TUBS-T (left) and UoM-B (right).

Figure 8 shows the residence time for all four analogues as well as a trendline indicating the theoretical time demand for other aperture sizes; note that the y-axis is on a logarithmic scale. All trendlines follow a power law of the form $f(x) = ax^{-k}$, with R^2 values between 0.9786 and 0.9976.

Results of the dry sieving experiment (Table 2 and Figure 8) show that choice of smaller sieve aperture sizes increase residence times for the experiment drastically. Thus, there is a careful trade off needed when selecting sieve aperture sizes for lunar sample processing mechanisms. It also shows that some of the particle size requirements for certain processes (Table 1) are difficult to achieve by dry sieving without manual sieve manipulation or large sieve shakers even in a terrestrial setting. Therefore, when developing new ISRU processes it is imperative to keep the necessary regolith pre-processing (i.e., sieving) requirements in mind. Additional testing performed with twice as much starting regolith simulant material (400 g) also showed clearly, that the quantity of material sieved at once (for an equivalent sieve area) should be kept to a minimum; an example of this can be seen in Figure 9. Once there is too much overhead (i.e., regolith simulant/analogue) in the sieve, which becomes consolidated due to the vibrations, the particles at the interface with the mesh cannot move sufficiently to orientate themselves in a way that would allow them to pass the sieve apertures. This results in passing percentages that are significantly lower than expected or drastically increased residence times (see Figure 9). Where the increase of screen area or decrease of batch size is not feasible, one solution to this problem could be the use of an additional soil agitation device, such as a rotating paddle or a wiper across the sieve surface, but this increases the complexity drastically (Singh, 2004). This could, however, also help to clean the sieving plates after use. In the present experiments, vibrations with a large acceleration and low frequency were applied (see Section 4.1, for details), as this vibration mode was able to provide the necessary agitation of particles to allow for an efficient separation given the provided mass of analogue material. For more detailed discussions of the relation between

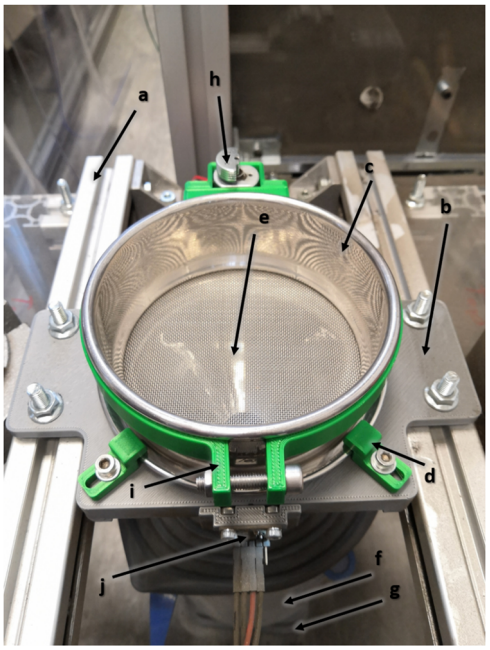

FIGURE 6 Experimental setup for the dry gravitational sieving of different regolith analogue materials. The aim of this experiment was to investigate a feasible aperture size for use in the proposed mechanism. Individual components are: (a) extruded aluminum profiles, (b) 3D-printed platform, (c) standard 100 mm diameter woven-wire mesh test sieve, (d) 3D-printed clamps, (e) funnel (underneath sieve), (f) weighing container, (g) scale with beam loadcell, (h) vibration motor, (i) 3D-printed collar for vibration motor, (j) 3-axis accelerometer [Color figure can be viewed at wileyonlinelibrary.com]

amplitude, frequency, and passing probability (see Katarzyna et al., 2016; Kudrolli, 2004; Lawinska & Modrzewski, 2017; Li & Tong, 2015).

Therefore, to increase the screening efficiency of a vibrating sieve the vibration profile needs to be optimised. Even though such optimisation is out of the scope of this study, as the induced vibration profile is inherit to a specific set-up (domain dependent), a set of experiments was operated with two vibrating motors in different orientations. For this, a second identical vibrating motor was attached to the platform (for set-up see Figure 6), rotated 90 degrees from the other motor. Both motors were operated at the same voltage and, therefore, frequency and acceleration. The test was performed with TUBS-M regolith simulant and the results can be seen in Table 3. Figure 10 shows the acceleration profiles for (a) the one-motor set-up and (b) the two-motor set-up.

Figure 10 shows that the use of two motors in different orientations lead to a roughly twofold increase on average maximum acceleration for the prevalent vibrational axis; due to the different orientation, this could not be assumed a given. More importantly, since the vibrations were induced at different locations, soil particles would constantly be in movement and would, therefore, have more chances of meeting a large enough aperture in the sieve (no areas of unagitated soil = good de-blinding). Table 3 shows that this reduces residence times significantly, as particles move horizontally as well as vertically across the screen, with the time savings becoming less prominent with a smaller aperture size. Thus, it is apparent that the vibration profiles of similar set-ups or mechanisms intended for the

TABLE 2 Overview of all performed dry sieving experiments including the used simulants, total analogue mass, aperture size of the used sieves, total duration of the experiment until the end condition was met, the coarse mass, the fine mass, the lost mass, the percentage passed, and the theoretical percentage passed based on the reported particle size distribution

Material	Mass [g]	Aperture size [µm]	Residence time [s]	Mass coarse [g]	Mass fine [g]	Mass lost [g]	Percentage passed [%]	PSD passing [%]
UoM-B	200	500	44.4	0.2	199.7	0.1	99.85	100
		250	410.1	0.6	198.8	0.6	99.40	99
		125	6545.8	21.1	178.4	0.5	89.20	88
Hess Pumice	200	500	167.9	0.0	198.7	1.3	99.35	100
		250	1614.7	0.3	199.4	0.3	99.70	99
		125	**23,662.0**					**84**
TUBS-M	200	1600	132.9	0.3	199.0	0.7	99.50	98
		1000	407.4	14.1	184.6	1.3	92.30	95
		800	600.0	20.4	179.8	0.0	89.90	93
		500	1005.7	26.2	173.8	0.0	86.90	87
		250	3847.4	48.9	151.0	0.1	75.50	75
TUBS-T	200	1600	66.1	0.8	199.0	0.2	99.50	98
		1000	715.9	12.5	186.1	1.4	93.05	95
		800	924.6	16.0	182.7	1.3	91.35	93
		500	4896.5	27.9	171.5	0.6	85.75	87
		250	**31,250.0**					**75**

Note: Bold values in Table shows experiments the residence time exceeded sensible time frames and thus the values were interpolated based on the percentage theoretically passing due to the particle size distribution (PSD) of the material.

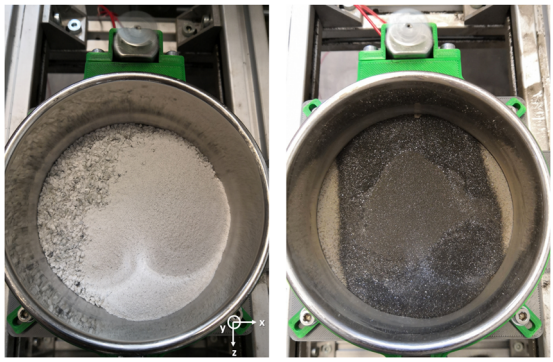

FIGURE 7 TUBS-T (left) and UoM-B (right) lunar regolith analogues during the dry sieving experiments. Axis directions of accelerometer indicated [Color figure can be viewed at wileyonlinelibrary.com]

use on the lunar surface, need to be well characterised and subsequently optimised for each specific mission requirement; a task which complexity must not be underestimated.

5 | LES^3 LABORATORY TESTS AND PERFORMANCE CHARACTERISTICS

Based on the results explained in Section 4, for the application in LES^3, a single vibrating motor (Figure 2 features g and k) is used at this proof-of-concept stage, however, a second motor could easily be incorporated on the opposite side of the inlet. However, for future deployment a smaller motor should be incorporated into the inlet structure; for more details see Section 6. Based on the previous dry sieving experiments (Section 4), a grain size

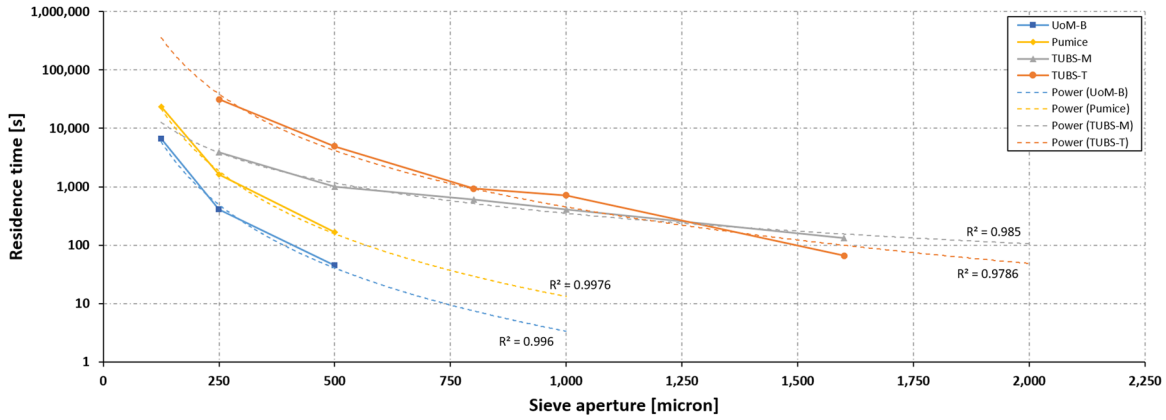

FIGURE 8 Residence time of different analogue materials during the gravitational dry sieving experiments. Trendlines represent a power law and R^2 values are displayed. Note the logarithmic scale of the *y*-axis [Color figure can be viewed at wileyonlinelibrary.com]

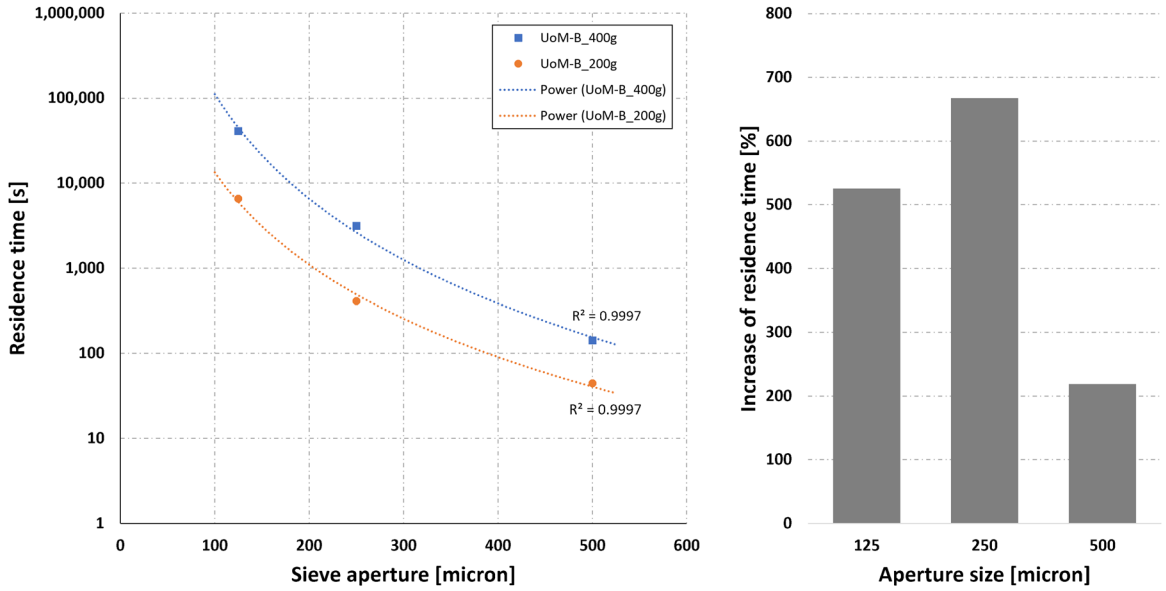

FIGURE 9 Residence times for 200 vs. 400 g of UoM-B analogue material during the dry sieving test. R^2 values of the power trendlines are displayed. The bar chart on the right shows the percentage increase in residence time based on the aperture size of the sieve, when the amount of sieved material was doubled from 200 to 400 g [Color figure can be viewed at wileyonlinelibrary.com]

TABLE 3 Comparative results of sieving experiments using one or two vibrating motors and TUBS-M regolith analogue

Mass [g]	No. of motors	Aperture size [µm]	End time [s]	Mass coarse [g]	Mass fine [g]	Mass lost [g]	Percentage passed [%]	Time difference [%]
200	1	1000	407.4	14.1	184.6	1.3	92.30	
	2		203.6	14.3	184.5	1.2	92.25	−50.03
	1	800	600.0	20.4	179.8	0.0	89.90	
	2		327.9	19.9	180.5	−0.4	90.25	−45.36
	1	500	1005.7	26.2	173.8	0.0	86.90	
	2		667.4	25.4	175.0	−0.4	87.50	−33.64
	1	250	3847.4	48.9	151.0	0.1	75.50	
	2		2965.0	45.3	154.9	−0.2	77.45	−22.94

Note: The total analogue mass, aperture size of the sieves, total duration of the experiment until the end condition was met, the coarse mass, the fine mass, the lost mass, the percentage passed, and the time difference compared to the same experiment with one motor is listed.

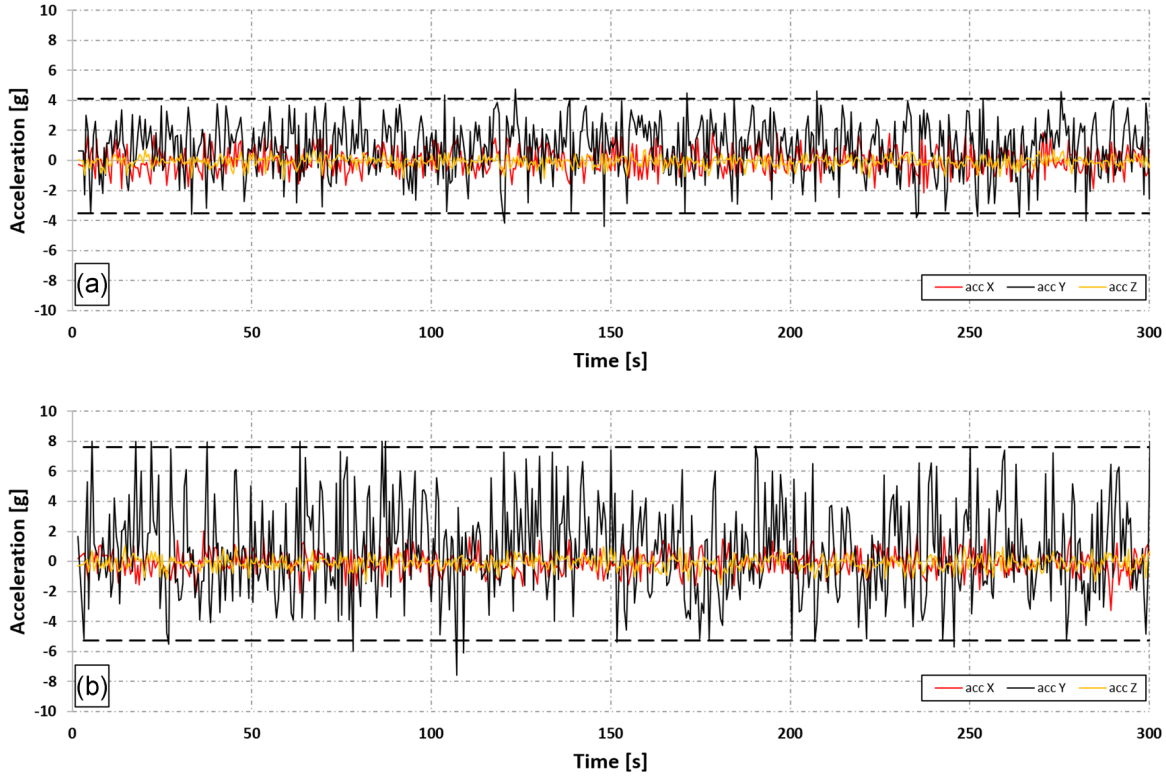

FIGURE 10 Acceleration profiles for dry sieving experiments with (a) one vibration motor and (b) two vibration motors. Dashed lines indicate the average (20) maximum/minimum acceleration of the most prominent vibrational axis (*y*-axis). Nominal acceleration of one motor (stand-alone) at 2.5 V was 4.5 g, as per datasheet. Axes directions can be seen in Figure 7 [Color figure can be viewed at wileyonlinelibrary.com]

separation down to 500 microns seems feasible in the two-stage separation process, and a pre-separation (Figure 2 feature b) of 1 mm was targeted. In the following, the results of the testing campaign in an analogue testbed at the University of Manchester will be reported.

The experimental setup of the analogue testbed at the University of Manchester was described by the authors before and can be found in detail in Just et al. (2021). The only change made was a new support structure to accompany the LES^3 mechanism. The experimental procedure for acquiring the horizontal excavation forces as well as the resetting of the soil bed after a sample collection run remained unchanged from Just et al. (2021) and will not be discussed again. Due to the geometry and operating principle of the mechanism, vertical excavation forces were not recorded. Tests were performed in three different settings, namely without a front sieving plate (i.e., sieve), with a 1 mm sieving plate, and with a 2 mm sieving

TABLE 4 Overview of all performed experimental run with the prototype in a large-scale analogue testbed

Mesh size [mm]	F_{H_max} 1 cm [N]	Mass [g]	F_{H_max} 1 cm (vib) [N]	Mass [g]	F_{H_max} 2 cm [N]	Mass [g]	F_{H_max} 2 cm (vib) [N]	Mass [g]	F_{H_max} 3 cm [N]	Mass [g]	F_{H_max} 3 cm (vib) [N]	Mass [g]
None	2.46	N.A.	1.94	N.A.	4.72	N.A.	3.98	N.A.	7.48	N.A.	6.47	N.A.
1 mm	1.00	34.2	1.46	52.4	3.82	68.1	2.78	80.0	6.67	75.0	6.55	93.4
2 mm	1.75	41.0	0.97	50.5	4.06	59.6	3.74	80.1	7.48	79.0	6.29	100.0

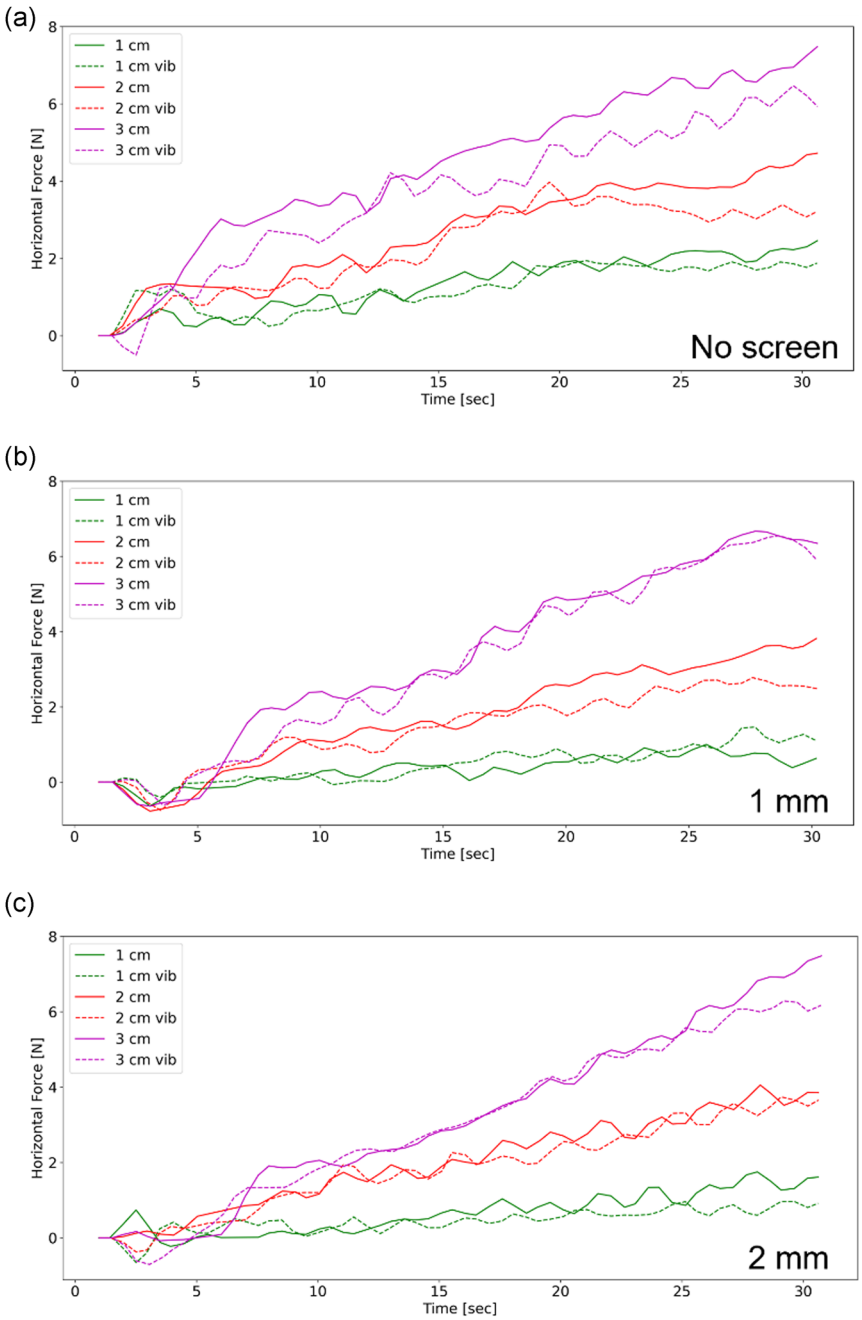

FIGURE 11 Necessary horizontal excavation forces for the experiments detailed in Table 4 with different front sieving plates (a–c) [Color figure can be viewed at wileyonlinelibrary.com]

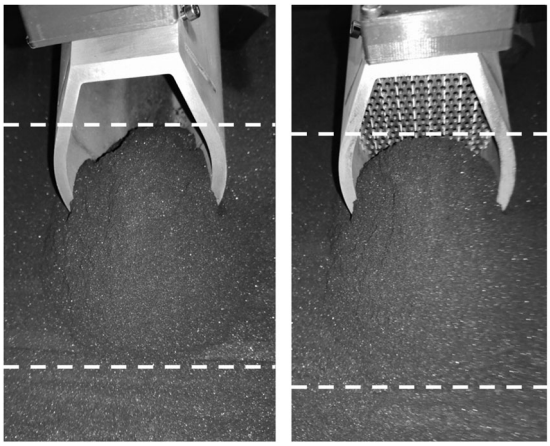

FIGURE 12 Qualitative comparison of the surcharge at 1 cm digging depth between no front screen (left) and a 2 mm front screen (right). Dashed lines indicate the surcharge and show that the surcharge length in front of the inlet is shorter for no screen, but that material advances further into the mechanism in this case

plate and at digging depths of 1–3 cm; runs were performed both with and without operation of the vibration motor. The use of vibrations is a proof-of-concept, and the optimisation of the vibrational profile is subject of future work. Here, the motor was operated at 2 V, translating into a maximum acceleration of 3.25 g and a frequency of 75 Hz. The cutting angle of the inlet was set to 15 degree and verified with a digital inclinometer (15° ± 0.5°). The excavation speed was set at 10 mm/s, as this yielded good results in prior experiments performed by the authors (Just et al., 2021). The operating procedure followed the steps described in Section 3.2 closely and the total mass acquired during the scoop was measured by capturing both size fractions for the runs with meshes. For the runs without the use of a mesh, which can be seen as a reference measurement in comparison with the forces recorded by the authors in Just et al. (2021), this would have not made sense due to the operating principle of the mechanism, which includes a screen for size separation. Table 4 shows all experimental runs, the maximum horizontal excavation force F_{H_max}, as well as the excavated mass. The distance traveled by the inlet through the sandbox was 31 cm for each run, resulting in an experiment time of around 31 s.

Figure 11 (features a–c) shows the necessary horizontal excavation force profiles for the experiments detailed above.

We observe that the overall excavation forces are several times lower than the traction force provided by the rover (~20 N on the lunar surface; Just et al., 2021), crucial for the mechanism to operate successfully (Table 4 and Figure 11). The run without a front sieving plate displays the highest maximum forces overall across all runs, as here the material enters the inlet relatively unhindered (i.e., no screening out of any particle sizes), leading to a shorter surcharge length and advancement of material further into the inlet. Thus, the most material of all runs has to be displaced in this instance. Without a screen, there is less build-up of surcharge in front of the inlet, but rather a larger build-up inside the inlet, and, therefore, the recorded force values are not directly proportional to the mass increase. A qualitative comparison of the surcharges with no screen and a 2 mm screen at 1 cm digging depth can be seen in Figure 12. The use of vibration facilitates the leading edge cutting through the soil, with a force reduction of up to 17 %. When comparing the runs with 1 mm and 2 mm sieving plates in front of the inlet, respectively, it becomes apparent that the required forces are relatively similar despite the different screens. Even though the values for the 2 mm mesh in Table 4 are slightly higher for most runs, this is usually less than 1 N, which in the present context, is insignificant. This similarity in forces can be assessed positively here, as a finer mesh does not seem to produce more surcharge. This will, of course change if one would try to pre-separate with a very small aperture size (i.e., sub-millimetre) for the considered particle sizes; this, however, does not align with the purpose of this mechanism and its operating principle. Generally, it can be seen that vibrations reduce the overall necessary excavation forces with observed reductions up to 30 %; this result is in good agreement with the results reported by the authors before Just et al. (2021). However, one should keep in mind that with the very low forces required for the shallow digging depth (below 1.5 N), even heterogeneities in the analogue substrate being excavated can cause a significant difference in overall force requirements. For example, agglutinated particles, rock fragments, or a locally compacted area of increased relative soil density. Overall, the obtained results prove the viability of the mechanism and demonstrate its applicability to the presented objectives.

A concern which is prevalent when using sieves is blinding or clogging of screens, subsequently reducing screening efficiency and increasing residence times. Due to the, for terrestrial sieves, relatively large aperture size and the operating procedure (Section 3.2) no significant impact of this phenomena on the separation performance has been observed. Tests during the standardised sieving test have shown an increase in residence time when the sieve is not cleaned in between runs, however, the vibration motor in combination with the possibility of tilting the mechanism downwards offers a way of removing stuck particles. A shearing mechanism or bursts of compressed gas could further facilitate this (Section 6) (Singh, 2004).

Table 5 shows an overview of the mass and preliminary power budget of the mechanism. The mass is differentiated between the mechanism mass and the mass of the camera with its moving platform, since the camera assembly mass is optional and mainly depending on the used lens, which is readily exchangeable. Even though the camera increases the capabilities of the mechanism, it is not required for the successful operation of LES^3. Peak power consumption occurs when all stepper motors are moving simultaneously, and the vibrating motor is in operation. Idle power consumption refers to the steppers merely holding their position.

As mentioned in Section 2, LES^3 must be considered as a mechanism designed for the LUVMI-X rover platform in the support of ISRU applications, where contamination of the material collected from different sampling sites is not too problematic. This application is intended by design and the support of analytical applications, such as the use of mass spectrometers, was not the driver for the

Total mass [g]	Mass camera (optional) [g]	Peak power consumption [W]	Idle power consumption [W]	Peak camera power consumption [W]
1985	200	6.5	3	3

TABLE 5 Overview of the mass and power budget of the proposed mechanism.

development. During the laboratory test campaign, material got trapped in several locations which led to an overall material loss of 3–4%, but did not cause any operational detractors. Some possible changes to reduce this lost fraction can be found in Section 6.

6 | SUMMARY

The presented work introduces a mechanism capable of combining regolith excavation with its beneficiation in the form of grain size separation. Since LES^3 is intended for use with a small and lightweight lunar rover, LUVMI-X (Garcet et al., 2019; Losekamm et al., 2021), minimising the required excavation forces is crucial. Laboratory tests in an analogue testbed have validated the working principle of the system and have shown that the mechanism, which mass is below 2 kg, is capable of excavating up to 100 g of soil in a single scoop while keeping the excavation forces at its maximum excavation depth of 3 cm below 8 N—around 40% of the traction force provided by the rover under lunar conditions. To facilitate size separation, LES^3 utilises a two-stage vibrating screen system. To investigate the feasibility of this system, an additional stand-alone dry sieving experiment was performed (Section 4) to identify a realistic separation level and to inform the operating requirements of gravitational vibrating size separation of regolith. It was shown that residence times scale with a power law when the aperture size is reduced. Thus, decreasing the necessary maximum particle size must be well justified. Furthermore, it is shown that batch sizes during vibrational sieving should be kept low (or sieve area maximized), as additional surcharge inside the sieve hinders the movement of particles and thus decreases separation efficiency. It is acknowledged that such size separation techniques can become challenging when applied in the low-gravity environment of the Moon and that the soil characteristics of regolith, especially its cohesion (Mitchell & Houston, 1972), pose another challenge; challenges which cannot be simulated here on Earth, as even the best simulants do not resemble the lunar regolith closely enough in all characteristics (Taylor et al., 2016). However, where a rough separation of particles by size is required and cross-contamination of sampling sites is not problematic, the presented system offers a simple way of achieving excavation and regolith grain size separation. We, therefore, are able to propose an alternative approach that eliminates an intermediate regolith conveying step and is significantly simpler than more advanced separation methods like electrostatic or magnetic separation (Higashiyama & Asano, 1998; Rasera et al., 2020; Trigwell, Captain, et al., 2013; Trigwell, Lane, et al. 2013). As many of the current ISRU processes rely on or benefit from a more controlled regolith feedstock (see Section 1), any level of particle size control will improve product quality and reduce the risk of ISRU process failure. Validation of the mechanism in a lunar gravity environment in the form of discrete element method (DEM) simulations, as well as how the sieving performance changes with reduced gravity, is subject of future work.

To further improve the capabilities of the mechanism, the following areas should be addressed and improved:

- **Dustproofing:** Currently, the mechanism has exposed actuators, sensors, and optical surfaces. For application on the lunar surface, the stepper motors, where space-certified models must be implemented, must be dust-proofed to minimise the risk of failure and the implementation of mitigation techniques against the highly electrostatic properties of regolith must be considered. The same is valid for the motors of the pan/tilt platform on which the camera sits, which lens also must be protected from a dust cover of the regolith. An enclosure for the whole cam/follower system seems feasible, which would eliminate the risk of a jammed slider preventing the discharge of material.
- **Material selection:** As mentioned above, the LES^3 lab prototype is manufactured from aluminum due to its ease of machining and low financial implications, with some parts having been anodized to increase wear resistance. However, for a future version of LES^3, different parts of the excavator will be manufactured from different materials. Whereas the inlet and the sieving plates must be made from a strong and wear-resistant material, other parts, such as the sliding doors, must be manufactured from a material with low sliding friction against the inlet material. In general, the use of coatings to reduce wear and keep granular material from sticking to surfaces seems beneficial and should be explored. The deployment of materials in a space environment and the connected challenges (e.g., radiation, thermal environment) must be considered and the space verification of all materials ensured.
- **Sensor/actuator selection:** The utilised vibrating motor, which facilitates both excavation and size separation, will be housed within the inlet structure at a suitable location. To maximise the scientific use of the mechanism, additional sensors could easily be integrated. This includes a loadcell to record the forces experienced by the inlet, a flow sensor to determine the flow rate of material inside the arm, and potentially an agitation system to increase sieving efficiency (as discussed in Section 4). This could, for instance, be a rotating paddle, but also small bursts of a compressed gas, where the latter could also be used to clean the sieving plates.
- **Mass reduction and dead volume:** To reduce launch mass as much as possible and free up maximum payload capacity on the rover, the overall mass of the system must be further reduced, which will require FEM analyses of all parts and subsequent mass

minimization. This is partly dependent on the mass of excavated and processed material required by the ISRU processes that are being supported in the given mission scenario, since this determines the scale of the inlet as well as the arm. Areas that can accumulate soil during operation must be minimized by design and mitigation methods implemented.

- **Test on the rover platform at analogue site and with icy regoliths:** To further evaluate the applicability of this prototype and due to the proposed polar deployment zone of LUVMI-X (Garcet et al., 2019; Losekamm et al., 2021), tests with icy regoliths or analogues prepared to comparable strength should be performed (Gertsch et al., 2006, 2008; Pitcher et al., 2016). Additionally, the mechanism is intended for a field analogue test with the rover in late 2021.

In summary, it was shown that the development of a dedicated excavation mechanism, targeting the readily powdered regolith top layer, with size separation capabilities for a lightweight lunar rover seems feasible. With an available traction force on the lunar surface of only around 20 N, engineering the mechanism for minimum excavation forces was crucial and implemented successfully. With several agencies as well as an increasing number of private companies currently developing small robotic vehicles for lunar applications, the design approach demonstrated in this study is applicable to the future development of excavation and beneficiation systems in the 100 s of grams range and emphasizes the need for specialized lunar excavation mechanisms once more. It also shows that, while being a discrete excavation method, low excavation forces are achievable during bulldozing motions, if the mechanism is specifically designed for it. The presented system can be utilised while the rover is moving and does not require the vehicle to stop (like other excavation mechanism; for instance, back hoes). The development of LES^3 also shows that, where powdered bulk regolith is required, focusing excavation activities to the top centimetres of soil simplifies the process due to limited effects of the changing regolith properties with depth.

ACKNOWLEDGMENTS

We appreciate the collaboration with Space Applications Services, who have provided valuable input for the development of the mechanism and this publication. Special thanks to Stefan Linke of the University of Braunschweig (Germany) for providing the TUBS analogue materials for this study. Gunter H. Just acknowledges the support of the University of Manchester's EPSRC Doctoral Training Partnership, ESA's Network & Partnership Initiative (4000130229/20/NL/MH/hm), and by the FAIR-SPACE Hub (RN0344). Katherine H. Joy is supported by the Science and Technology Facilities Council (ST/R000751/1), the Royal Society (URF\R\201009), and the Leverhulme Trust (RPG-2019-222). M. J. Roy acknowledges support from the EPSRC (EP/L01680X/1) through the Materials for Demanding Environments Centre for Doctoral Training, as well as the FAIR-SPACE Hub (RN0344). K. L. Smith acknowledges support from the FAIR-SPACE Hub (RN0344). Lastly, we want to thank the reviewers of this documents for the valuable comments which increased the quality of this manuscript.

CONFLICT OF INTERESTS

The authors declare that there are no conflict of interests.

DATA AVAILABILITY STATEMENT

The data that support the findings of this study are available from the corresponding author upon reasonable request.

ORCID

Gunter H. Just http://orcid.org/0000-0001-9924-2605
Matthew J. Roy http://orcid.org/0000-0002-6558-4903
Katherine H. Joy http://orcid.org/0000-0003-4992-8750
Katharine L. Smith http://orcid.org/0000-0001-7471-0708

REFERENCES

Allan, S. M., Merritt, B. J., Griffin, B. F., Hintze, P. E., & Schulman, H. S. (2013). High-temperature microwave dielectric properties and processing of JSC-1AC lunar simulant. *Journal of Aerospace Engineering*, *26*, 874–881.

Altun, A. A., Ertl, F., Marechal, M., Makaya, A., Sgambati, A., & Schwentenwein, M. (2021). Additive manufacturing of lunar regolith structures. *Open Ceramics*, *5*, 100058.

Anand, M., Crawford, I. A., Balat-Pichelin, M., Abanades, S., Van Westrenen, W., Péraudeau, G., Jaumann, R., & Seboldt, W. (2012). A brief review of chemical and mineralogical resources on the Moon and likely initial in situ resource utilization (ISRU) applications. In: *Planetary and Space Science* (pp. 42–48).

ASTM International. (2020). E11-20: Standard specification for woven wire test sieve cloth and test sieves.

Balasubramaniam, R., Gokoglu, S., & Hegde, U. (2010). The reduction of lunar regolith by carbothermal processing using methane. *International Journal of Mineral Processing*, *96*, 54–61.

Balla, V. K., Roberson, L. B., O'Connor, G. W., Trigwell, S., Bose, S., & Bandyopadhyay, A. (2012). First demonstration on direct laser fabrication of lunar regolith parts. *Rapid Prototyping Journal*, *18*, 451–457.

British Standard Institution. (2000). BS 410-1:2000, ISO 3310-1:2000: Test sieves—Technical requirements and testing—Part 1: Test sieves of metal wire cloth.

Burns, J. O., Duric, N., Taylor, G. J., & Johnson, S. W. (1990). Observatories on the Moon. *Scientific American*, *262*, 42–49.

Carpenter, J. D., Fisackerly, R., & Houdou, B. (2016). Establishing lunar resource viability. *Space Policy*, *37*, 52–57.

Cesaretti, G., Dini, E., De Kestelier, X., Colla, V., & Pambaguian, L. (2014). Building components for an outpost on the lunar soil by means of a novel 3D printing technology. *Acta Astronautica*, *93*, 430–450.

Chavers, D. G., Ess, K., Moore, J., Dervan, M., Ondocsin, W., Carson, J. M., & Johnson, W. (2016). NASA Lander Technologies Project Status. In *AIAA SPACE* 2016 (p. 5221).

Cockell, C. S. (2010). Astrobiology—what can we do on the moon? *Earth, Moon, and Planets*, *107*, 3–10.

Colwell, J. E., Batiste, S., Horanyi, M., Robertson, S., & Sture, S. (2007). Lunar surface: Dust dynamics and regolith mechanics. *Reviews of Geophysics*, *45*, RG2006.

Crawford, I. A. (2004). The scientific case for renewed human activities on the Moon. *Space Policy*, *20*, 91–97.

Crawford, I. A. (2015). Lunar resources: A review. *Progress in Physical Geography*, *39*, 137–167.

Crawford, I. A., Anand, M., Cockell, C. S., Falcke, H., Green, D. A., Jaumann, R., & Wieczorek, M. A. (2012). Back to the Moon: The scientific rationale for resuming lunar surface exploration. *Planetary and Space Science*, *74*, 3–14.

Crawford, I. A., Elvis, M., & Carpenter, J. D. (2016). Using extraterrestrial resources for science. *Astronomy & Geophysics*, *57*, 32–36.

Crawford, I. A., & Joy, K. H. (2014). Lunar exploration: Opening a window into the history and evolution of the inner solar system. *Philosophical Transactions of the Royal Society A: Mathematical Physical and Engineering Sciences*, *372*, 20130315.

Crawford, I. A., & Zarnecki, J. (2008). Astronomy from the Moon. *Astronomy and Geophysics*, *49*, 17–19.

Delgado, A., & Shafirovich, E. (2013). Towards better combustion of lunar regolith with magnesium. *Combustion and Flame*, *160*, 1876–1882.

Ellery, A. (2018). Lunar in situ resource utilisation—the key to human salvation on Earth. In: *Earth and Space* (pp. 380–389).

Fateri, M., & Gebhardt, A. (2015). Process parameters development of selective laser melting of lunar regolith for on-site manufacturing applications. *International Journal of Ceramic Technology*, *12*, 46–52.

Fateri, M., Gebhardt, A., & Khosravi, M. (2013). Experimental investigation of selective laser melting of lunar regolith for in-situ applications. In *ASME International Mechanical Engineering Congress and Exposition, Proceedings* (IMECE) 2A.

Garcet, J., Urbina, D., Sheridan, S., Biswas, J., Evagora, A., Richter, L., Fau, G., Kumar, H., Fodorcan, D., Chupin, T., Kullack, K., Pitcher, C., Murray, N., Reiss, P., Reganaz, M., Govindaraj, S., Aked, R., & Salini, J. (2019). Lunar volatiles mobile instrumentation (LUVMI) project results. In: *70th International Astronautical Congress* (IAC) IAC-19-A3.2C.6.

Gatsonis, N. A., Lu, Y., Blandino, J., Demetriou, M. A., & Paschalidis, N. (2016). Micropulsed plasma thrusters for attitude control of a low-earth-orbiting cubesat. *Journal of Spacecraft and Rockets*, *53*, 57–73.

Gertsch, L., Gustafson, R., & Gertsch, R. (2006). Effect of water ice content on excavatability of lunar regolith. *AIP Conference Proceedings*, *813*, 1093–1100.

Gertsch, L., Rostami, J., & Gustafson, R. (2008). Review of Lunar regolith properties for design of low power Lunar excavators. In *6th International Conference on Case Histories in Geotechnical Engineering* (pp. 1–15).

Goulas, A., Binner, J. G. P., Engstrøm, D. S., Harris, R. A., & Friel, R. J. (2019). Mechanical behaviour of additively manufactured lunar regolith simulant components. *Proceedings of the Institution of Mechanical Engineers, Part L: Journal of Materials: Design and Applications*, *233*, 1629–1644.

Goulas, A., Binner, J. G. P., Harris, R. A., & Friel, R. J. (2017). Assessing extraterrestrial regolith material simulants for in-situ resource utilisation based 3D printing. *Applied Materials Today*, *6*, 54–61.

Goulas, A., & Friel, R. (2016). 3D printing with moondust. *Rapid Prototyping Journal*, *22*, 864–870.

Gustafson, R. J., White, B. C., & Fidler, M. J. (2011). Oxygen production via carbothermal reduction of Lunar regolith. *SAE International Journal of Aerospace*, *4*, 311–316.

Hadler, K., Martin, D. J. P., Carpenter, J., Cilliers, J. J., Morse, A., Starr, S., Rasera, J. N., Seweryn, K., Reiss, P., & Meurisse, A. (2020). A universal framework for space resource utilisation (SRU). *Planetary and Space Science*, *182*, 104811.

Higashiyama, Y., & Asano, K. (1998). Recent progress in electrostatic separation technology. *Particulate Science and Technology*, *16*, 77–90.

Hintze, P. E., & Quintana, S. (2013). Building a lunar or martian launch pad with in situ materials: Recent laboratory and field studies. *Journal of Aerospace Engineering*, *26*, 134–142.

Ishimatsu, T., de Weck, O. L., Hoffman, J., & Ohkami, Y. (2016). Generalized multicommodity network flow model for the earth-moon-mars logistics system. *Journal of Spacecraft and Rockets*, *53*, 25–38.

Jakus, A. E., Koube, K. D., Geisendorfer, N. R., & Shah, R. N. (2017). Robust and elastic lunar and martian structures from 3D-printed regolith inks. *Scientific Reports*, *7*, 44931.

Jaumann, R., Hiesinger, H., Anand, M., Crawford, I. A., Wagner, R., Sohl, F., Jolliff, B. L., Scholten, F., Knapmeyer, M., Hoffmann, H., Hussmann, H., Grott, M., Hempel, S., Köhler, U., Krohn, K., Schmitz, N., Carpenter, J., Wieczorek, M., Spohn, T., … Oberst, J. (2012). Geology, geochemistry, and geophysics of the Moon: Status of current understanding. *Planetary and Space Science*, *74*, 15–41.

Jester, S., & Falcke, H. (2009). Science with a lunar low-frequency array: From the dark ages of the Universe to nearby exoplanets. *New Astronomy Reviews*, *53*, 1–26.

Joy, K. H., Crawford, I. A., Curran, N. M., Zolensky, M., Fagan, A. F., & Kring, D. A. (2016). The Moon: An archive of small body migration in the Solar System. *Earth, Moon, and Planets*, *118*, 133–158.

Joy, K. H., Kring, D. A., Bogard, D. D., Mckay, D. S., & Zolensky, M. E. (2011). Re-examination of the formation ages of the Apollo 16 regolith breccias. *Geochimica et Cosmochimica Acta*, *75*, 7208–7225.

Just, G. H., Joy, K. H., Roy, M. J., & Smith, K. L. (2020a). Geotechnical characterisation of two new low-fidelity lunar regolith analogues (UoM-B and UoM-W) for use in large-scale engineering experiments. *Acta Astronautica*, *173*, 414–424.

Just, G. H., Roy, M. J., Joy, K. H., & Smith, K. L. (2021). Experimental Investigation of the Effect of Leading-edge geometry on Excavation Forces and their Reduction for Small-scale Continuous Lunar Excavators. *Journal of Aerospace Engineering Currently under review*.

Just, G. H., Smith, K. L., Joy, K. H., & Roy, M. J. (2020b). Parametric review of existing regolith excavation techniques for lunar in situ resource utilisation (ISRU) and recommendations for future excavation experiments. *Planetary and Space Science*, *180*, 104746.

Katarzyna, L., Remigiusz, M., & Piotr, W. (2016). Mathematical and empirical description of screen blocking. *Granular Matter*, *18*, 1–10.

Khoshnevis, B., Yuan, X., Zahiri, B., Zhang, J., & Xia, B. (2016). Construction by contour crafting using sulfur concrete with planetary applications. *Rapid Prototyping Journal*, *22*, 848–856.

Kobayashi, T., Ochiai, H., Fukagawa, R., Aoki, S., & Tamoi, K. (2006). A proposal for estimating strength parameters of lunar surface from soil cutting resistances. In *Earth and Space 2006—Proceedings of the 10th Biennial International Conference on Engineering, Construction, and Operations in Challenging Environments*. American Society of Civil Engineers (p. 63).

Kudrolli, A. (2004). Size separation in vibrated granular matter. *Reports on Progress in Physics*, *67*, 209–247.

Labeaga-Martínez, N., Sanjurjo-Rivo, M., Díaz-Álvarez, J., & Martínez-Frías, J. (2017). Additive manufacturing for a Moon village. *Procedia Manufacturing*, *13*, 794–801.

Larson, W. E., Sanders, G. B., & Hyatt, M. (2011). ISRU—From concept to reality: NASA accomplishments and future plans. *AIAA SPACE Conference and Exposition*, *2011*, 1–15.

Lasue, J., Wiens, R. C., Clegg, S. M., Vaniman, D. T., Joy, K. H., Humphries, S., Mezzacappa, A., Melikechi, N., McInroy, R. E., & Bender, S. (2012). Remote laser-induced breakdown spectroscopy (LIBS) for lunar exploration. *Journal of Geophysical Research: Planets*, *117*, 1002.

Lavoie, A. R., & Spudis, P. D. (2016). The purpose of human spaceflight and a lunar architecture to explore the potential of resource utilization. In *SPACE 2016 Conference & Exposition* (p. 5526).

Lawinska, K., & Modrzewski, R. (2017). Analysis of sieve holes blocking in a vibrating screen and a rotary and drum screen. *Physicochemical Problems of Mineral Processing*, *53*, 812–828.

Li, Z., & Tong, X. (2015). A study of particles penetration in sieving process on a linear vibration screen. *International Journal of Coal Science and Technology*, *2*, 299–305.

Lim, S., Prabhu, V. L., Anand, M., & Taylor, L. A. (2017). Extra-terrestrial construction processes—Advancements, opportunities and challenges. *Advances in Space Research*, *60*, 1413–1429.

Linke, S., Windisch, L., Kueter, N., Voss, A., Przwara, P., Grasshoff, M., Stoll, E., Schilde, C., & Kwade, A. (2018). TUBS-M and TUBS-T—New lunar regolith simulants adaptable to local surface characteristics. In *Proceedings of the International Astronautical Congress*, IAC (pp. 1–5).

Linne, D. L., Sanders, G. B., & Taminger, K. M. (2015). Capability and technology performance goals for the next step in affordable human exploration of space. In *8th Symposium on Space Resource Utilization* (pp. 1–14).

Lomax, B. A., Conti, M., Khan, N., Bennett, N. S., Ganin, A. Y., & Symes, M. D. (2020). Proving the viability of an electrochemical process for the simultaneous extraction of oxygen and production of metal alloys from lunar regolith. *Planetary and Space Science*, *180*, 104748.

Losekamm, M. J., Barber, S., Biswas, J., Chupin, T., Evagora, A., Fau, G., Fodorcan, D., Gancet, J., Kubitza, S., Madakashira, H. K., Murray, N., Neumann, J., Pöschl, T., Reganaz, M., Richter, L., Schröder, S., Schwanethal, J., Sheridan, S., Urbina, D., & Wessels, P. (2021). LUVMI-X: A versatile platform for resource prospecting on the Moon. In: *Earth and Space 2021: Space Exploration, Utilization, Engineering, and Construction in Extreme Environments - Selected Papers from the 17th Biennial International Conference on Engineering, Science, Construction, and Operations in Challenging Environments*. American Society of Civil Engineers (ASCE) (pp. 289–299).

Meurisse, A., Beltzung, J. C., Kolbe, M., Cowley, A., & Sperl, M. (2017). Influence of mineral composition on sintering Lunar regolith. *Journal of Aerospace Engineering*, *30*, 1–8.

Meurisse, A., Makaya, A., Willsch, C., & Sperl, M. (2018). Solar 3D printing of Lunar regolith. *Acta Astronautica*, *152*, 800–810.

Mitchell, J. K., & Houston, W. N. (1972). Mechanical properties of lunar soil. In *Proceedings of the Third Lunar Science Conference*.

Moore, H. J., Bickler, D. B., Crisp, J. A., Eisen, H. J., Gensler, J. A., Haldemann, A. F. C., Matijevic, J. R., Reid, L. K., & Pavlics, F. (1999). Soil-like deposits observed by Sojourner, the Pathfinder rover. *Journal of Geophysical Research: Planets*, *104*, 8729–8746.

Neal, C. R. (2009). The Moon 35 years after Apollo: What's left to learn? *Chemie der Erde*, *69*, 3–43.

Pelech, T. M., Sibille, L., Dempster, A., & Saydam, S. (2021). A framework for Off-Earth mining method selection. *Acta Astronautica*, *181*, 552–568.

Pitcher, C., Kömle, N., Leibniz, O., Morales-Calderon, O., Gao, Y., & Richter, L. (2016). Investigation of the properties of icy lunar polar regolith simulants. *Advances in Space Research*, *57*, 1197–1208.

Raju, M., Ponnada, M. R., Singuru, P., Engineering, C., Vijayram, M., & Raj, G. (2014). Advances in manufacture of Mooncrete—A review. *International Journal of Engineering Science & Advanced Technology*, 501–510.

Rasera, J. N., Cilliers, J. J., Lamamy, J.-A., & Hadler, K. (2020). The beneficiation of lunar regolith for space resource utilisation: A review. *Planetary and Space Science*, *186*, 104879.

Reddy, V. S. (2018). The SpaceX Effect. *New Space*, *6*, 125–134.

Sacksteder, K. R., & Sanders, G. B. (2007). In-situ resource utilization for lunar and mars exploration. In *Collection of Technical Papers—45th AIAA Aerospace Sciences Meeting* (Vol 6, 4232–4237).

Sanders, G. B. (2011). Comparison of lunar and Mars in-situ resource utilization for future robotic and human missions. In *49th AIAA Aerospace Sciences Meeting*.

Sanders, G. B., Larson, W. E., Sacksteder, K. R., & McLemore, C. A. (2008). NASA in-situ resource utilization (ISRU) project—development & implementation. In *AIAA SPACE 2008 Conference & Exposition*.

Sanders, G. B., Simon, T. M., Rosenbaum, B. J., Larson, W. E., Quinn, J. W., Captain, J. E., & Boucher, D. S. (2010). Overcoming the hurdles of incorporating In-Situ Resource Utilization (ISRU) into human lunar exploration. In *Proceedings of the 12th International Conference on Engineering, Science, Construction, and Operations in Challenging Environments—Earth and Space 2010* (pp. 1308–1325).

Sargeant, H. M., Abernethy, F. A. J., Barber, S. J., Wright, I. P., Anand, M., Sheridan, S., & Morse, A. (2020). Hydrogen reduction of ilmenite: Towards an in situ resource utilization demonstration on the surface of the Moon. *Planetary and Space Science*, *180*, 104751.

Schlüter, L., & Cowley, A. (2020). Review of techniques for in-situ oxygen extraction on the moon. *Planetary and Space Science*, *181*, 104753.

Sefton-Nash, E., Carpenter, J. D., Fisackerly, R., & Trautner, R., ESA Lunar Exploration Team, Prospect User Group, Prospect Industrial Team. (2018). PROSPECT: ESA's package for resource observation and in-situ prospecting for exploration, commercial exploitation, and transportation. In *49th Lunar and Planetary Science Conference* (p. 2083; id. 2740).

Sik Lee, T., Lee, J., & Yong Ann, K. (2015). Manufacture of polymeric concrete on the Moon. *Acta Astronautica*, *114*, 60–64.

Singh, R. (2004). Vibratory separators still make the grade for screening dry bulk powders. *Filtration and Separation*, *41*, 20–21.

Sitta, L. A. (2017). Study on feasibility of 3D printing with Moon highlands regolith simulant. *Politecnico di Milano*.

Song, X., Zhai, W., Huang, R., Fu, J., Fu, M., & Li, F. (2020). Metal-based 3D-printed micro parts & structures. *Reference Module in Materials Science and Materials Engineering*. Elsevier.

Spudis, P. D., Lavoie, & A. R. (2011). Using the resources of the Moon to create a permanent, cislunar space faring system. In: *AIAA SPACE 2011 Conference & Exposition*.

Sullivan, R., Anderson, R., Biesiadecki, J., Bond, T., & Stewart, H. (2011). Cohesions, friction angles, and other physical properties of Martian regolith from Mars Exploration Rover wheel trenches and wheel scuffs. *Journal of Geophysical Research*, *116*, E02006.

Sunshine, D. (2010). Mars science laboratory CHIMRA: A device for processing powdered martian samples. In: *Proceedings of the 40th Aerospace Mechanisms Symposium*. NASA Kennedy Space Center (pp. 249–262).

Taylor, L. A., & Meek, T. T. (2005). Microwave sintering of lunar soil: Properties, theory, and practice. *Journal of Aerospace Engineering*, *18*, 188–196.

Taylor, L. A., Pieters, C. M., & Britt, D. (2016). Evaluations of lunar regolith simulants. *Planetary and Space Science*, *126*, 1–7.

Taylor, S. L., Jakus, A. E., Koube, K. D., Ibeh, A. J., Geisendorfer, N. R., Shah, R. N., & Dunand, D. C. (2018). Sintering of micro-trusses created by extrusion-3-D-printing of lunar regolith inks. *Acta Astronautica*, *143*, 1–8.

Toutanji, H., Glenn-Loper, B., & Schrayshuen, B. (2005). Strength and durability performance of waterless lunar concrete. In *43rd AIAA Aerospace Sciences Meeting and Exhibit—Meeting Papers* (pp. 11427–11438).

Trigwell, S., Captain, J., Weis, K., & Quinn, J. (2013). Electrostatic beneficiation of lunar regolith: Applications in in situ resource utilization. *Journal of Aerospace Engineering*, *26*, 30–36.

Trigwell, S., Lane, J. E., Captain, J. G., Weis, K. H., Quinn, J. W., & Watanabe, F. (2013). Quantification of efficiency of beneficiation of lunar regolith. *Particulate Science and Technology*, *31*, 45–50.

Vogt, D., Schröder, S., Hübers, Heinz-Wilhelm Richter, L., Deiml, M., Glier, M., Weßels, P., & Neumann, J. (2020). VOILA on LUVMI-X: Volatiles detection in the Lunar polar region with laser-induced breakdown Spectroscopy. In: *Europlanet Science Congress 2020* (Vol. 14. pp. EPSC2020-780).

Vogt, D., Schröder, S., Hübers, H.-W., Richter, L., Deiml, M., Wessels, P., & Neumann, J. (2021). VOILA on LUVMI-X: A LIBS instrument for the detection of volatiles at the Lunar South Pole. In *EGU General Assembly 2021* (pp. EGU21-5906).

von Ehrenfried, M. (2020). Spacecraft, landers, rovers and payloads. In *The Artemis Lunar Program* (pp. 48–74).

Voosen, P. (2018). NASA to pay private space companies for moon rides. *Science*, *362*, 875–876.

Wen, P., Zheng, N., Nian, J., Li, L., & Shi, Q. (2015). Flux of granular particles through a shaken sieve plate. *Scientific Reports*, *5*, 1–9.

Werkheser, N. J., Fiske, M. R., Edmunson, J. E., & Khoshnevis, B. (2015). Development of additive construction technologies for application to development of lunar/martian surface structures using in-situ materials. In *CAMX 2015—Composites and Advanced Materials Expo* (pp. 2395–2402).

Wilkinson, A. (2011). Size beneficiation of regolith for simplicity and efficiency. In *Planetary and Terrestrial Mining and Sciences Symposium (PTMSS)*.

Williams, R. J., McKay, D. S., Giles, D., & Bunch, T. E. (1979). Mining and beneficiation of lunar ores. In *Space Resources and Space Settlements* (pp. 275–288).

Zhang, J., & Khoshnevis, B. (2015). Selective separation sintering (SSS) a new layer based additive manufacturing approach for metals and ceramics. In *Proceedings of Solid Freeform Fabrication Symposium* (pp. 71–79).

How to cite this article: Just, G. H., Roy, M. J., Joy, K. H., Hutchings, G. C., & Smith, K. L. (2021). Development and test of a Lunar Excavation and Size Separation System (LES^3) for the LUVMI-X rover platform. *Journal of Field Robotics*, 1–18. https://doi.org/10.1002/rob.22050